Cerebral Cortex, 2021;00: 1–12

https://doi.org/10.1093/cercor/bhab389
Original Article

ORIGINAL ARTICLE

Neuronal Electrical Ongoing Activity as Cortical Areas Signature: An Insight from MNI Intracerebral Recording Atlas

Karolina Armonaite[1], Massimo Bertoli[2,3], Luca Paulon[2], Eugenia Gianni[2,4], Marco Balsi[5], Livio Conti[6,7] and Franca Tecchio[2,†]

[1]Faculty of Psychology, Uninettuno University, Rome 00186, Italy, [2]Laboratory of Electrophysiology for Translational NeuroScience (LET'S), Institute of Cognitive Sciences and Technologies - Consiglio Nazionale delle Ricerche, Rome 00185, Italy, [3]Department of Neuroscience, Imaging and Clinical Sciences, University 'Gabriele D'Annunzio' of Chieti-Pescara, Chieti 66100, Italy, [4]Unit of Neurology, Neurophysiology, Neurobiology, Department of Medicine, Università Campus Bio-Medico di Roma, Rome 00128, Italy, [5]Department of Information Engineering, Electronics and Telecommunications, Sapienza University, Rome 00185, Italy, [6]Faculty of Engineering, Uninettuno University, Rome 00186, Italy and [7]INFN - Istituto Nazionale di Fisica Nucleare, Sezione Roma Tor Vergata, Rome 00133, Italy

Address correspondence to Franca Tecchio, LET'S – ISTC – CNR, via Palestro 32, 00185 Rome, Italy. Email: franca.tecchio@cnr.it
[†]All the correspondence can be sent to the corresponding author at franca.tecchio@cnr.it

Abstract

The time course of the neuronal activity in the brain network, the neurodynamics, reflects the structure and functionality of the generating neuronal pools. Here, using the intracranial stereo-electroencephalographic (sEEG) recordings of the public Montreal Neurological Institute (MNI) atlas, we investigated the neurodynamics of primary motor (M1), somatosensory (S1) and auditory (A1) cortices measuring power spectral densities (PSD) and Higuchi fractal dimension (HFD) in the same subject (M1 vs. S1 in 16 subjects, M1 vs. A1 in 9, S1 vs. A1 in 6). We observed specific spectral features in M1, which prevailed above beta band, S1 in the alpha band, and A1 in the delta band. M1 HFD was higher than S1, both higher than A1. A clear distinction of neurodynamics properties of specific primary cortices supports the efforts in cortical parceling based on this expression of the local cytoarchitecture and connectivity. In this perspective, we selected within the MNI intracortical database a first set of primary motor, somatosensory and auditory cortices' representatives to query in recognizing ongoing patterns of neuronal communication. Potential clinical impact stands primarily in exploiting such exchange patterns to enhance the efficacy of neuromodulation intervention to cure symptoms secondary to neuronal activity unbalances.

Key words: complexity, dynamics, electroencephalography (EEG), fractal dimension, oscillatory frequency bands

Introduction

The discovery by Nobel laureates Camillo Golgi (Golgi 1873) and Santiago Ramón y Cajal (Cajal 1888) of the existence of the neuron, the minimal constitutive unit of the brain, marked the birth of a plethora of neuroscientific disciplines. In the course of just over a century, largely enabled by an increasingly strong technological availability and computational capacity, the neuroscientific community has been able to access the complexity of the nervous system by shedding light on the mechanisms that determine both its structure and its functional organizational principles. It is nowadays shared that the human brain is a dynamic complex system made up of interacting

subcomponents shaped over multiple space–time scales (Bullmore et al. 2009; Bassett and Sporns 2017). Accordingly, brain functioning can be conceived in terms of a system of neuronal networks made of connected nodes, where the node can be a single neuron, a group of the same neurons, a region of local neurons or wide brain areas (Tecchio et al. 2020).

The scalp electroencephalography (EEG) results from the ongoing continuous fluctuation of the activity of thousands of neurons in response to excitatory and inhibitory projections (Lopes Da Silva 2011; Buzsáki and Watson 2012), detectable at scalp level as brain rhythmic activities distributed in several frequency ranges and associated with specific brain functions (Thut et al. 2012; Buzsáki et al. 2013). Analyzing local neuronal activity derived by EEG scalp data, previous results (Cottone et al. 2017) supported the hypothesis that each cortical area generates an electrical activity resulting in a specific time course, the local neurodynamics, that represents a signature of that area. The authors collected first indications that different and distinctive neuronal resting-state neurodynamics could represent a new coding for cortex parceling, prospectively complementing Brodmann's classification of the brain cortical areas based on cytological and topological evidence (Brodmann 1909).

EEG is the elective investigation tool for the noninvasive assessment of the local neurodynamics, as it directly senses the electrical activity of the brain, with the same proper temporal resolution of the neuronal electric exchanges. Since the seminal work by Hans Berger (Berger 1929), noninvasive EEG has provided access to a deep understanding of physiological and pathological features of brain activity and their behavioral correlates. In addition, intracranial stereo-encephalographic (sEEG) recordings, widely used in neuroscience investigations in animal models, enabed investigations in humans recording the brain electrical activity in patients with drug-resistant epilepsy. Notably, in accessing the regions of interest, the electrodes cross brain regions spared from the epileptogenic dysfunction, allowing us to access an extraordinarily wealth of information from relatively healthy brain zones (Frauscher et al. 2018).

Capitalizing on the multicentre data collection of sEEG dense coverage recordings in normal cortical regions, during open eyes wakefulness, made available by the world-renowned Montreal Neurological Institute (MNI) (Frauscher et al. 2018), the purpose of our study is to deepen knowledge of the brain neurodynamics as cortical area signature. Moving on from the noninvasive EEG-derived successful attempt to differentiate the neurodynamics of the primary somatosensory (S1) and motor (M1) hand representations (Cottone et al. 2017a), here we aim to strengthen the results by running a similar analysis on MNI sEEG assessments, extending the investigation to further primary cortical areas. Since primary visual areas were not available in the MNI database, we extended the study to primary auditory (A1) cortices.

Methods

Study Design

After selecting the available sEEG recordings within S1, M1, and A1, we investigated their local neurodynamics in terms of power spectrum and HFD (Higuchi 1988). Whenever diverse cortical areas expressed specific power spectra and/or HFD signatures, we evaluated whether a relationship existed between the two neurodynamics features by a correlation analysis (Fig. 1).

Data Selection

Intracranial Stereo-EEG Recordings

The intracranial EEG recordings were accessed through the open database (Fig. 2), published by MNI, available at https://mni-open-ieegatlas.research.mcgill.ca/main.php and presented in (Frauscher et al. 2018). The MNI dataset consists of 1785 intracranial EEG recordings, 1 min each, sampled at 200 Hz, and artifact free, detected at rest with closed eyes, from 106 patients diagnosed with refractory focal epilepsy (13–68 years old, 48 females) investigated by means of either cortical surface strip/grid or sEEG electrodes.

Our investigation focused selectively on primary cortices since they display the most repeatable behavior and are the most simple to label. In particular, (Cottone et al. 2017a) have shown that the neurodynamics indices displayed a clear and different pattern for diverse cortical parcels, specifically S1 and M1 areas, with no distinction between left and right sides, in all subjects. However, the distribution of the neurodynamics index in the entire population overlapped widely across cortical regions, S1 and M1 in the case of (Cottone et al. 2017b), with S1 ranging between 1.42 and 1.81 and M1 between 1.43 and 1.82. This means that by randomly sampling the available population, our observations would lose the regularity of the relationship that exists at the individual level between the fractal dimensions of S1 and M1. In order to be sensitive to the true relationship of the neurodynamics of the different cortical areas, in the present article we adopted the most conservative approach by selecting only recordings from subjects who were studied in at least two of the areas of interest: A1 & M1, A1 & S1, S1 & M1. The available sEEG recordings within primary cortical areas (Fig. 3) are constituted by: 50 channels for S1, 99 for M1 and 18 for A1.

Homogenous Weighting of the Subjects by Selecting an Individual Representative Channel

Although for some subjects, only a single channel in a region of interest was available, in some cases multiple channels were available for the same region (Table 1). To weight all subjects homogenously, we identified a criterion for selecting a single representative channel for each region for every subject. Noteworthy, the present work grounds our future perspective of studying the temporal structures typical of local neuronal pools and their exchanges across brain regions. For such an aim, we need the identification of a representative of each cortical area of interest, with its ongoing neurodynamics. In fact, averages can be obtained for indices, as we did to enhance the confidence in the selection of the representative, but cannot be used for obtaining a more reliable description of the local ongoing time course.

The criterion we used was mainly based on the electrode's location along the three regions of our interest, through the spatial coordinates provided in MNI data. Given the M1 and S1 anatomical proximity, we first select the M1 and S1 representatives as belonging to counterparts to the same body part representation. To do this, we selected the S1 and M1 representatives detected in locations with the minimum

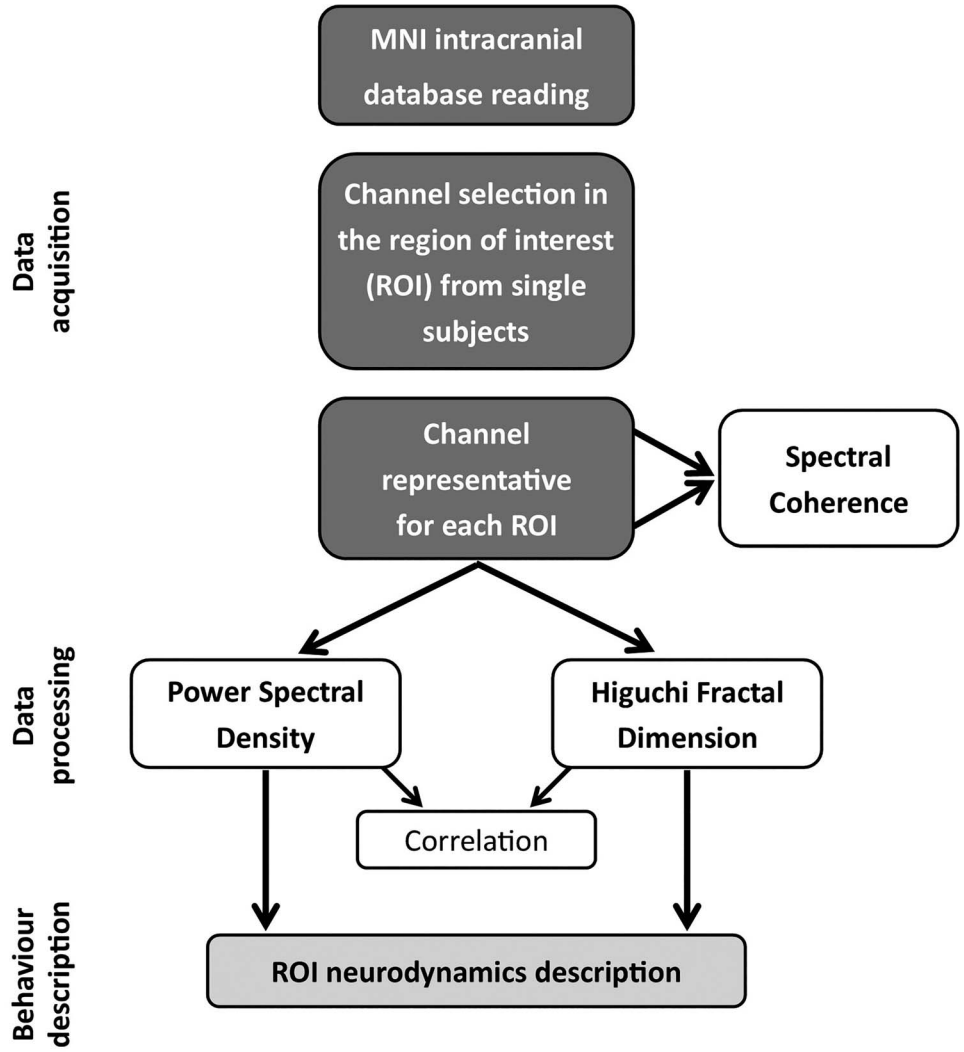

Figure 1. Study flowchart. Flowchart is divided into three sections separated with different shades. Arrows indicate a direct one-sided connection of two blocks. The case where the two arrows are surjected into a single block (i.e., Spectral Coherence) signifies that the estimation needs of an involvement of more than one ROI.

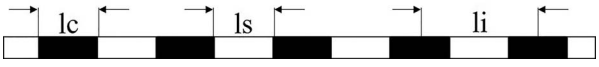

Figure 2. Recording electrode. Representation of a portion of a Dixi electrode adopted in the majority of the MNI channels investigated, with the typical dimensions: length of contact (lc) ~ 2 mm, distance between consecutive contacts (ls) ~ 1.5 mm, resulting distance between the centres of two contacts (li) ~ 3.5 mm. The total exploration length depends on the number of contacts of an electrode varying from 5 to 18 in the studied recordings.

difference in z coordinate (points at fixed z define the axial plane) and *x* coordinate (fixed *x* defines the coronal plane); and we selected the most frontal position available (greater *y* values) for M1 than S1 (smaller *y* values, moving along sagittal plane). If, for a subject, none of the multiple channels fulfilled this criterion, we arbitrarily selected as representative the channel which showed the most typical behavior in the power spectra (Fig. 4). For A1, we selected as representative channel the one in the most central position among those available.

Neurodynamics Analysis

In the MNI, each sEEG channel is provided subdivided into segments, with a time length of at least 5 s, and we gave care to assess quantitative indices in windows excluding the discontinuities.

In order to identify the neurodynamics features, characteristic of the 3 investigated regions, we considered 2 approaches: the estimate of the spectral analysis and the fractal dimension of the studied signals.

To support the suitability of representative selection, we also included the description of the avarage across all channels in each individual.

Spectral Features

To extract the spectral properties of the signal, we calculated the PSD of each representative channel. We applied a Hamming tapering to the time series and evaluated the Fast Fourier Transform on sequences of 256 samples each (about 1.28 s, obtaining a frequency resolution of ~0.78 Hz) with a sliding

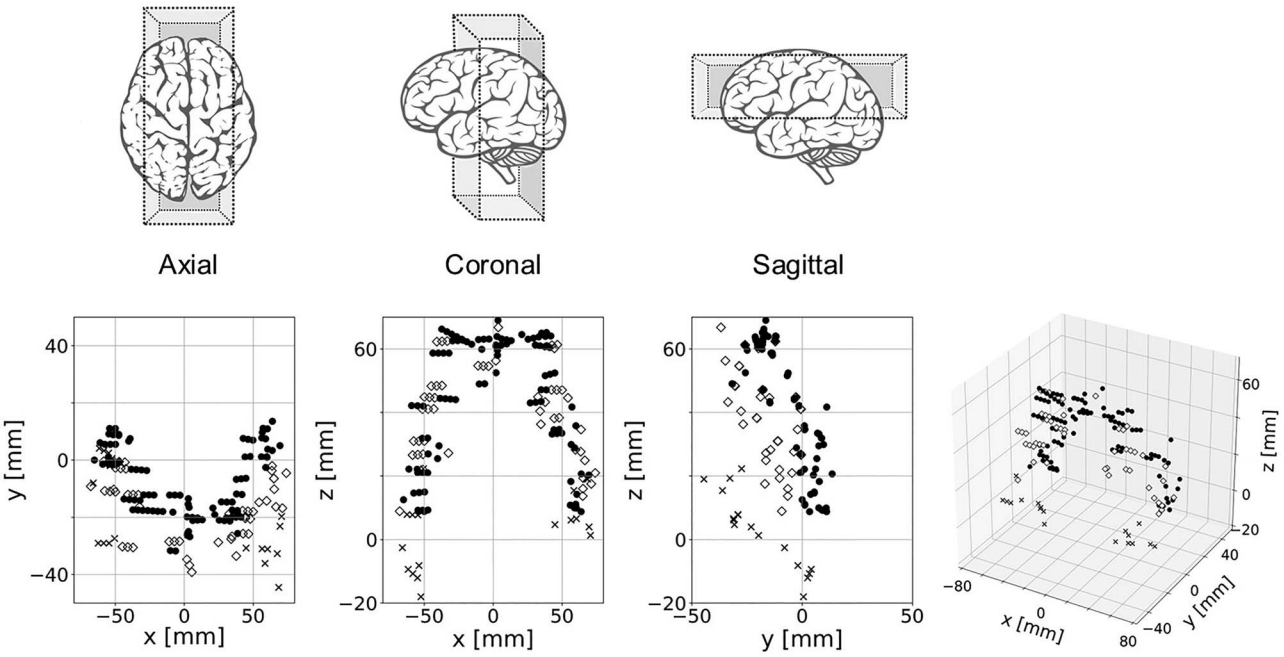

Figure 3. Exploring spatial distribution of MNI channels of the regions of interest. Representation of channels position in the orthogonal projections for the 21 subjects having data collected in at least two regions of interest, among A1 (crosses), S1 (empty diamonds), and M1 (filled circles). The *x* axis is oriented from left to right, *y* axis from back to front and *z* from bottom to top. As schematized on top of the figure, on the left panel the axial plane direction of the head is presented with the projection of channel positions in the represented volume, in the middle panel the coronal plane direction and on the right one the sagittal plane direction. Rightmost, the representation of the same channels position in 3D space.

window overlap of 50% according to the Welch method. PSD values are normalized so that the area under each curve is equal to 1.

According to the bandpass filter of the MNI database proper for the used sampling frequency, the maximum frequency available was 80 Hz. We categorize the spectrum from 0.5 Hz to 80 Hz into 7 frequency bands: delta [≤3 Hz], theta [4-7 Hz], alpha [8-12 Hz], low beta [13-25 Hz], high beta [26-32 Hz], low gamma [33-48 Hz] and high gamma [49-80 Hz]. For each subject, the PSD in a single band is calculated as the integral of normalized power within the band divided by the number of frequency bins.

Higuchi's Fractal Dimension

In continuity with (Cottone et al. 2017a), we estimated the fractal dimension of the sEEG signals as defined by Higuchi, who developed an algorithm working in the time domain, without the need of using the frequency representation (Higuchi, 1988).

According to the concept of quantifying the emergence of similar features at different time scales, Higuchi's algorithm uses many time series built by down-sampling the original signal X(i) (with $i = 1, \ldots, N$) every k samples:

$$X_k^m = \left\{ X(m), X(m+k), X(m+2k), \ldots, X(m+((N-m)/k)k) \right\}$$

where k is a constant integer value ($1 < k \leq K_{max}$) with $K_{max} < N/2$ and $m = 1, 2, 3, \ldots, k$.

Then the length $L_m(k)$ of the curve X_k^m is defined as the average value over k-1 sets of $X_m(k)$ as follows:

$$L_m(k) = \left[\left(\sum_{i=1}^{\mathrm{int}\left(\frac{N-m}{k}\right)} |X(m+ik) - X(m+(i-1)k)| \right) \frac{N-1}{\mathrm{int}\left(\frac{N-m}{k}\right)k} \right] \frac{1}{k}$$

If $L(k) \approx k^{-HFD}$, then the curve is fractal with dimension equal to HFD.

Although HFD is a property of the signal independent of the amplitude of the signal and the estimating window's length, the HFD estimate depends on the single parameter K_{max}. In this framework, we estimated the HFD at the value of K_{max} where its value starts stabilizing, namely $K_{max} = 35$, fixed across all subjects and the three areas (Fig. 5).

Statistical Analysis

In each fixed frequency band, the values of PSD on the population displayed non-normal distribution as quantified by the Shapiro–Wilk test. Similarly, the distribution of HFD values between subjects was not Gaussian. Thus, to compare HFDs and PSDs of pairs of cortical sources of all subjects, we deployed the nonparametric Wilcoxon test (hereafter W_{test} values), which uses the ranking method of differences. The test was applicable for comparing S1 and M1 functional sources, as their match had enough subjects. In the case of A1 versus S1 and M1, we provided a descriptive evaluation, without applying statistical comparisons, due to the low number of subjects.

Table 1 Summary of selected channels

ID	Age	Sex	S1			M1			A1		
			#Chs	Channel name	Scaler (V)	#Chs	Channel name	Scaler (V)	#Chs	Channel name	Scaler (V)
5	27	M	1	GD005Lw_5W	1.42E-4	2	GD005Lx_5W	2.32E-4	-	-	-
7	40	F	4	GD007Rz14W	5.83E-4	11	GD007Rf9W	4.94E-4	3	GD007Rt5W	1.62E-4
9	28	M	1	GD009Rj12W	3.93E-4	10	GD009Rj08W	2.22E-4	-	-	-
13	23	F	-	-	-	3	GD013Lr_13W	3.52E-4	1	GD013Lu_8W	7.08E-4
16	19	F	2	GD016Rj11W	3.38E-4	4	GD016Rb10W	6.20E-4	-	-	-
18	41	M	-	-	-	8	GD018Ln_03W	5.05E-4	3	GD018Lt_05W	2.06E-4
23	19	M	1	GD023Rz12W	2.34E-4	2	GD023Rh13W	6.61E-4	-	-	-
26	17	M	13	GD026Li_14W	8.36E-4	11	GD026Lm_2W	2.69E-4	-	-	-
29	35	M	2	GD029Ri12W	4.62E-4	13	GD029Rh11W	2.33E-4	1	GD029Rd10W	2.19E-4
34	41	M	-	-	-	3	GD034Lr_6W	2.83E-4	3	GD034Lu_5W	1.73E-4
37	23	F	1	GD037Lr_5W	1.55E-4	-	-	-	1	GD037Ls_5W	1.19E-4
44	24	F	3	GD044Lh_11W	1.61E-4	2	GD044Lq_6W	1.90E-4	-	-	-
45	51	M	3	GD045Rf7W	5.06E-4	2	GD045Rf5W	2.20E-4	-	-	-
47	23	F	6	GD047Ln_11W	1.11E-3	8	GD047Lm_11W	5.25E-4	-	-	-
93	25	M	3	NG093RF143W	3.62E-5	2	NG093RF144W	2.57E-5	1	NG093RF121W	4.45E-5
94	18	F	2	NG094RF42W	3.61E-4	3	NG094RF43W	3.13E-4	-	-	-
98	13	F	3	NA098RP81W	2.70E-4	5	NA098RP42W	3.06E-4	2	NG098RG26W	3.87E-4
99	41	M	1	NG099RG230W	3.19E-4	3	NG099RG228W	3.05E-4	-	-	-
100	24	M	1	NG100RG31W	2.60E-4	4	NG100RG29W	3.72E-4	1	NG100RT68W	2.06E-4
103	24	F	-	-	-	1	NG103LG145W	2.24E-4	2	NG103LT14W	3.84E-4
110	27	F	3	NG110RG614W	3.84E-4	2	NG110RG613W	3.21E-4	-	-	-

For each of the 21 subjects included in the study (having recordings in at least two regions of interest S1, M1 and A1) the table reports: MNI ID, age, sex, total number of available channels in each region, name of the representative channel selected for this study and the scaling factor needed to normalize the channel amplitude to [−1,1]. In total we have: 99 channels for M1, 50 for S1 and 18 for A1. Channel name coding: second letter indicates the type of electrode (D for Dixi, A for AdTech and G for grid), the three digits before the L/R hemisphere label represent the patient ID whereas the next alphanumerical string denotes the contact identification and the last letter (W) indicates the state, as all data are collected in wake condition. In agreement with Frauscher *et al.* (2018a), it is possible to compare signals collected with different type of electrodes.

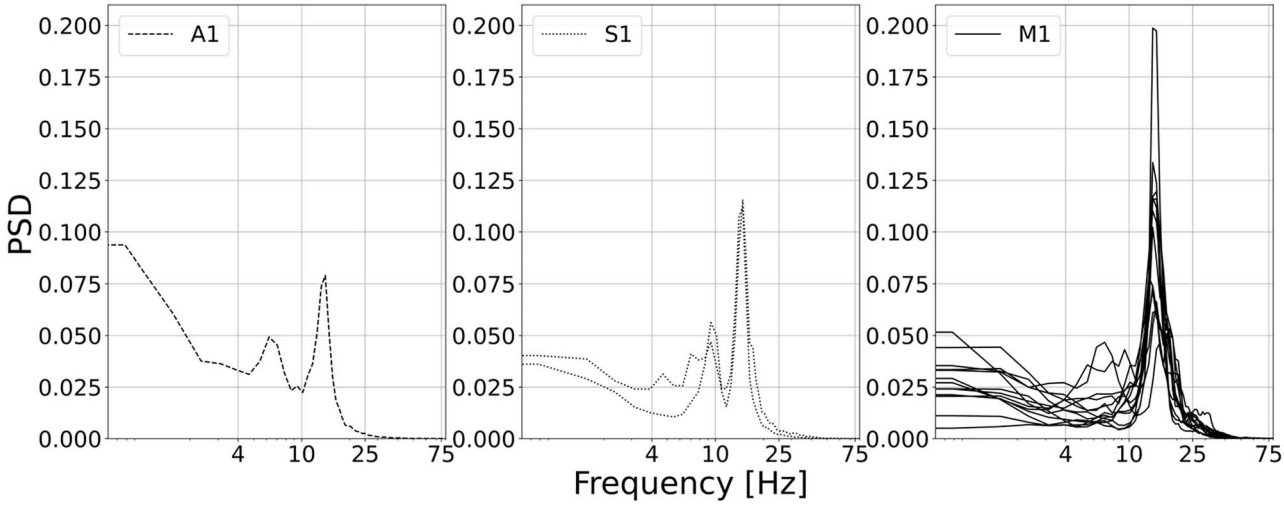

Figure 4. Local neurodynamics: Power Spectra Density (PSD). Example of power spectra density as a function of frequency in subject 29, who had one channel in A1 (left, dashed line), 2 channels in S1 (middle, dotted line) and 13 channels in M1 (right, continuous line). PSD values are normalized so that the area under each curve is equal to 1.

To investigate the possible relationship between HFD and PSD in different areas and frequency bands, we assessed their Pearsons' correlation coefficient and its statistical significance.

Cortico-Cortical Functional Connectivity

Even though our work is focused on the local neurodynamics, which mirrors cytoarchitecture of the involved cortical parcel and its projections to and from the whole brain, we also exploited the availability of synchronous recordings in the regions of interest to have an idea about their functional connectivity. We measured it via spectral coherence, by using the same estimate parameters as PSD, in 5 people among the 3 regions, as they have the recordings in the 3 areas, and in couples of regions (16 subjects for the couple S1-M1, 9 for A1-M1 and 6 for A1-S1).

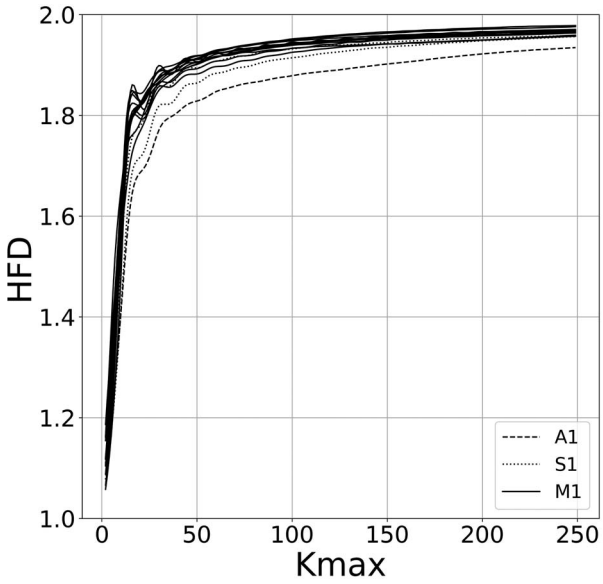

Figure 5. Local neurodynamics: Higuchi fractal dimension as a function of K_{max}. Example of HFD as a function of K_{max} for subject 29. Multiple curves refer to different channels available for this subject for the studied regions.

Results

By applying the constraint of having one recording of at least 2 cortical regions in each subject—independently of the hemisphere—we have 21 subjects (11 males and 10 females, Table 1). The mean age was 27.8 ± 9.9 years, similarly distributed across sex. Among them, 20 subjects had M1 recordings, 17 had S1 and 10 had A1. The neurodynamics comparison was possible in 16 subjects for the couple S1-M1, 9 for A1-M1 and 6 for A1-S1 (5 subjects had recordings for all 3 areas).

Power Spectrum

Local neurodynamics appeared specific for cortical parcels in terms of PSD band values (Fig. 6A and 7 Left): S1 consistently showed greater power than M1 in alpha band [$W_{test} = 26, P = 0.03$] and smaller in high beta [$W_{test} = 25$, $P = 0.03$], low gamma [$W_{test} = 15$, $P = 0.01$] and high gamma [$W_{test} = 28$, $P = 0.04$]. A1 had power in delta frequency band greater than M1 (9 out of 9 subjects) whereas smaller in low beta (7/9), high beta (7/9) and low gamma (7/9) bands. A1 steadily showed greater power than S1 in the delta band (6/6) and smaller in low (5/6) and high beta (4/6) bands.

In order to support our findings obtained by using representative channels, we evaluated the differences among the three primary cortices (A1, S1, and M1) also by using the PSD value averaged across all channels of each subject (Fig. 6C). In complete agreement with the results obtained on representatives, PSD of M1 was greater than that of S1 in high beta [$W_{test} = 19$, $P = 0.01$], low gamma [$W_{test} = 19$, $P = 0.01$], and high gamma [$W_{test} = 27$, $P = 0.03$] bands. Whereas PSD of A1 is greater than S1 and M1 in delta band in all subjects, PSD of A1 is lower than that of S1 in low beta 6(6) and high beta 6(6) as well as that of M1 in low beta 8(9), high beta 8(9), and low gamma 8(9) bands.

Fractal Dimension

By using a representative for each subject, the HFD of M1 was consistently greater than S1 for each subject [$W_{test} = 12, P = 0.01$] (Fig. 6B and 7 Right), and A1 HFD was smaller than HFD for S1 and M1 regions.

Moreover, by using HFD (evaluated at $K_{max} = 35$) averaged across all channels in each subject (Fig. 6D), we obtained the same results as for representative channels, namely HFD of M1 is higher than in S1 [$W_{test} = 28$, $P = 0.04$] and HFD of A1 is lower than in S1 and M1 with 5(6) and 8(9), respectively.

Correlation between Fractal Dimension and Power Spectrum Density

By using the representative approach, we have investigated the correlation between HFD and PSD over the whole population, as depicted in Table 2. HFD negatively correlated ($P < 0.001$) with PSD of low-frequency bands delta (A1), theta (S1 and M1), and alpha (S1), whereas HFD typically correlated positively with the PSD of beta in A1 and PSD of high-frequency bands beta and gamma for S1 and M1.

We also studied the correlation between HFD and PSD in all 7 bands, evaluated starting from the interchannel averages in each subject. Consistently with the results for representative channels, we observe that low-frequency bands such as delta negatively correlate with HFD of A1, and theta with HFD of S1 and M1 (Table 2). Moreover, positive correlations with HFD were noticed in the beta band for all three regions and for S1 as well as M1 in low gamma bands. The high gamma band positively correlated only with HFD of S1.

Cortico-Cortical Functional Connectivity

We observed that, as expected from brain structure and function, the coherence between S1 and M1 is higher than the coherence of these two regions with A1 across the whole spectrum (see Fig. 8).

Discussion

The core result of this study is to have highlighted, within a large variability across subjects (Fig. 9), the existence of

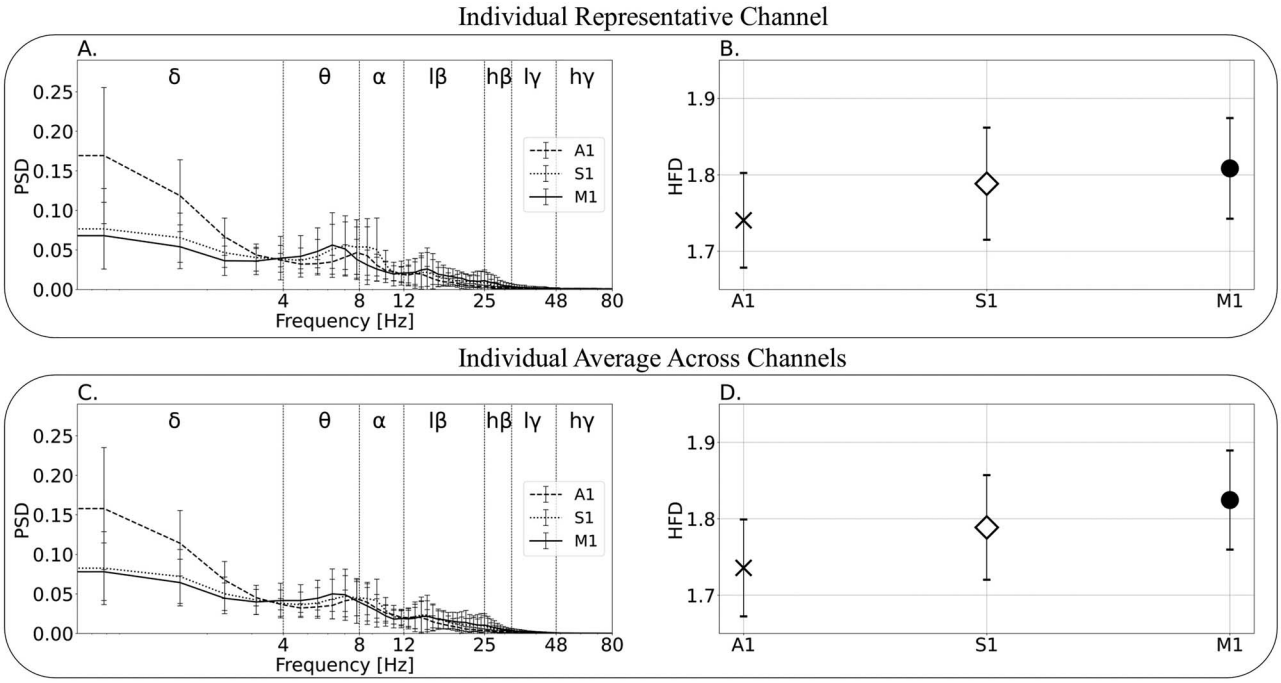

Figure 6. Mean of the spectral and fractal neurodynamics indices of the A1, S1 and M1 areas. Panels A and B show the mean (and standard deviation) of PSD and HFD, respectively, estimated across population, as a function of frequency. For each subject we considered a representative of all available channels within the A1, S1, and M1 regions. The Higuchi fractal dimension was evaluated at $K_{max} = 35$. Plots of panels C and D show the same, but using for each subject the average of all applicable channels.

Table 2 Correlation across population of HFD and PSD

			Delta	Theta	Alpha	Low beta	High beta	Low gamma	High gamma
Representative channel	**A1** (10 subjects)	***r***	**−0.86**	0.57	0.40	**0.79**	0.61	0.47	0.23
		P	**0.00**	0.09	0.25	**0.01**	0.06	0.17	0.51
	S1 (17 subjects)	***r***	−0.21	**−0.82**	**−0.51**	**0.82**	**0.82**	**0.71**	**0.61**
		P	0.43	**0.00**	**0.04**	**0.00**	**0.00**	**0.00**	**0.01**
	M1 (20 subjects)	***r***	−0.23	**−0.84**	−0.19	**0.53**	**0.60**	**0.65**	**0.52**
		P	0.34	**0.00**	0.43	**0.02**	**0.00**	**0.00**	**0.02**
Mean over channels	**A1** (10 subjects)	***r***	**−0.80**	0.51	0.24	**0.86**	**0.67**	0.53	0.27
		P	**0.01**	0.13	0.50	**0.00**	**0.04**	0.11	0.44
	S1 (17 subjects)	***r***	−0.32	**−0.90**	−0.17	**0.78**	**0.76**	**0.70**	**0.64**
		P	0.21	**0.00**	0.52	**0.00**	**0.00**	**0.00**	**0.01**
	M1 (20 subjects)	***r***	**−0.47**	**−0.79**	−0.27	**0.74**	**0.60**	**0.58**	0.39
		P	**0.04**	**0.00**	0.24	**0.00**	**0.01**	**0.01**	0.09

Pearson's coefficient (*r*) and significance (*P*) of the correlation across population between the HFD value and the PSD in different bands. HFD and PSD have been evaluated from representative channel in each subject (above) and by averaging over all channels in each subject (below). Significant results are bolded.

typical features of the time course of the electrical activity of diverse cortical parcels. The second relevant result is to have derived from the MNI database a set of primary cortices' representatives to be interrogated with appropriate artificial intelligence tools or other algorithmic approches to develop new models for cortex parceling based on the neuronal pools' neurodynamics.

Local Neurodynamics

Local PSD

One of the main results achieved by the present investigation concerns the identification of a compact index of local neurodynamics peculiar for different cortical regions as a candidate for a novel cortical parceling method enriching the well-established cytoarchitecture of cortical brain areas.

Our investigation of the primary motor, somatosensory, and auditory cortex cortices revealed spectral behaviors in good agreement with the differentiation described at whole-brain lobes level in (Frauscher et al. 2018). In fact, we observed M1, S1, and A1 spectral features with the PSD beta and gamma prevalence in the frontal lobe, alpha in the parietal lobe, and delta in the temporal lobe (see horizontal segments in Fig. 4A of Frauscher et al. 2018, Supplementary Material).

Local Fractal Dimension

The neuroscientific community—by investigating at multiscale the dynamical structure of local and global neural networks,

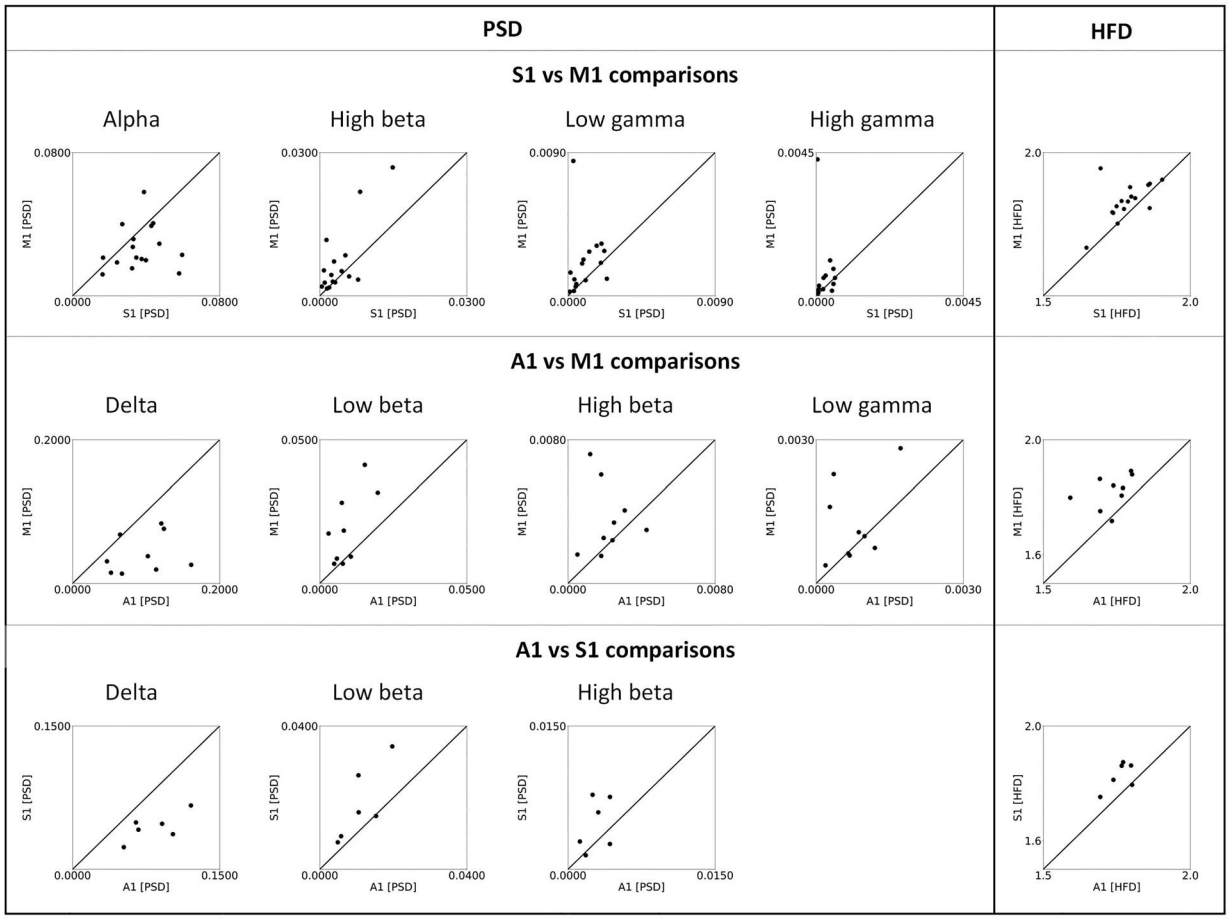

Figure 7. Local neurodynamics comparison. Left rectangle: for comparing the neurodynamics of the studied brain areas couples, the scatterplots (between subjects) of the PSD band values are shown for the frequency bands where the two sources differ such as: S1 versus M1 [16 subjects] in 4 bands; A1 versus M1 [9 subjects] in 4 bands; A1 versus S1 [6 subjects] in 3 bands. Right rectangle: scatterplots of HFD between subjects for each couple of brain areas. In each plot, a point above (below) the diagonal has a PSD band value of the source represented on *x* axis lower (higher) than that of the source shown on *y* axis. Similarly, for the HFD scatterplots.

and connecting those dynamics to biophysical mechanisms and cognitively important computations—clearly agrees that, even in resting-state, the neuronal activity time course is nonstationary and nonlinear (Kopell et al. 2014). This means that the EEG signal can display patterns of organization that recur at different magnitudes generating fractal properties (Di Ieva et al. 2014). Investigating the neurodynamics, the time course of neuronal electrical activity, we selected the fractal dimension index, aware of the existence at different scales of self-similar regularities in the signal, that are distributed according to a scale-free behavior, thus following a power-law distribution (Buzsáki and Mizuseki 2014). Accordingly, grounding on existing knowledge, we proposed a unique functional organizing principle—the feedback-synchrony-plasticity triad—which, governing the neuronal networks at multiple scales, emerges as a potential explanatory framework for the fractal properties exhibited by neurodynamics (Tecchio et al. 2020). The fractal dimension of EEG signals has proven to be a reliable marker of underlying neuronal electrical activity, sensitive to alterations in clinical scenarios such as stroke (Zappasodi et al. 2014), Alzheimer's disease (Smits et al. 2016), and fatigue in multiple sclerosis (MS) (Porcaro et al. 2019).

Higher Motor than Sensory Cortex Complexity

Here, in agreement with previous results from noninvasive EEG investigation (Cottone et al. 2017a), we corroborated the evidence that the fractal dimension of M1 activity is larger than S1. The analysis, extended to the primary auditory area, also indicated a smaller fractal dimension of A1 compared with both S1 and M1.

It is therefore possible to interpret this newly strengthened finding in the evolutionary perspective, where cortical areas have developed their structure and functionality in accordance with the requirements posed by the environment, developing a functional hierarchy within primary motor cortices' activities. As the ideation, execution and monitoring of whatever behavioral outcome emerges from M1 directed to muscular effectors, this cortical area undertakes the more sophisticated functional role (Wolpert et al. 2011) with respect to the single processes' steps that regulate sensory perception, mirroring its higher dexterity into higher signal fluctuation richness quantified by higher fractal dimension. In this same direction, we can interpret the higher fractal dimension of S1 than A1 activity. In fact, although auditory information is crucial for the interaction with the environment, somatosensory and proprioceptive feedback

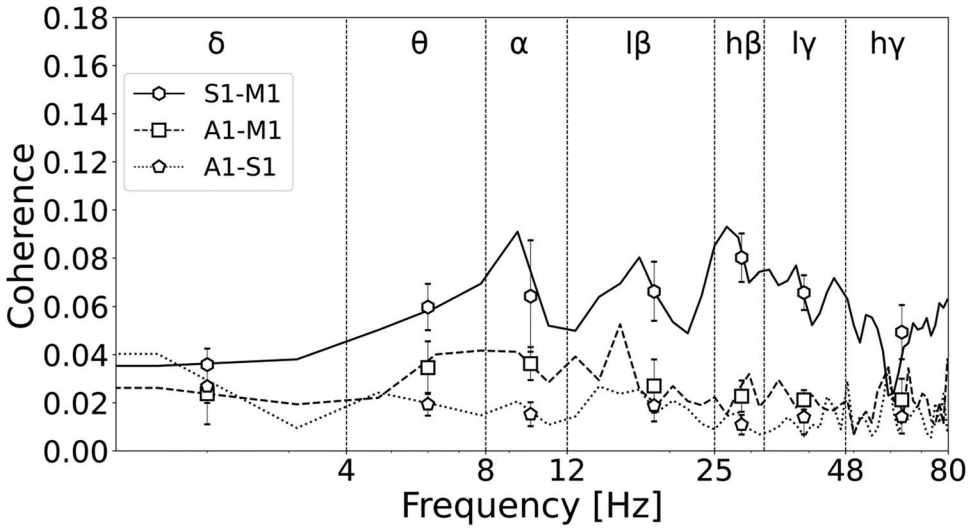

Figure 8. Cortico-cortical functional connectivity. Spectral coherence between couples of cortical parcels averaged across population plot as a function of frequency. We show the mean and the standard deviation across corresponding frequency bands.

constitutes a building block of motor control itself. On the same line, given the predictive function of gaze with respect to the motor realization (Johansson et al. 2001), there are indications that the fractal dimension of the activity of primary visual cortical areas shows values even higher than those of primary sensorimotor (Marino et al. 2019). It could be the aim of future work, to verify, as suggested by our model and observed by (Marino et al. 2019), whether in the MNI intracortical EEG database the neuronal activities of the secondary and associative cortices have lower fractal dimension than those of primary ones.

Spectral Versus Fractal Dimension Relationship

Noteworthy, the correlative analysis between power spectra and HFD revealed that HFD is suitable in summarizing in a single index the different spectral features of the probed cortical areas activities. This relationship between fractal dimension and power spectra emerged stably from multiple scalp EEG data studies (Zappasodi et al. 2014, 2015; Smits et al. 2016; Cottone et al. 2017a) is strengthened by the present intracortical sEEG investigation.

Resting-State Neurodynamics

We observed, as the Gotmans' group did, that even in resting-state with closed eyes, different brain regions exhibit specific neuronal electrical activity characteristics (Frauscher et al. 2018). To date, brain activity at rest is not considered as the result of random fluctuations (Fox and Raichle 2007) but rather as reflecting, in its organization, the behavioral potential of the generating structures (Deco et al. 2011; Lin et al. 2020). In the context of error prediction models that look at the enactment of complex behaviors as the result of prediction and feedback mechanisms (Friston 2010; Clark 2016), the opportunity to qualify and describe the characteristics of resting-state brain activity provides a fundamental tool for understanding the mechanisms that underpin the brain state in healthy or pathological conditions (Spetsieris et al. 2015; Damborská et al. 2019).

This is especially true in the context of chronic diseases or symptoms that are primarily driven by a pathological alteration of neuronal electrical activity (Gianni et al. 2021; Razza et al. 2021). In this regard, promising indications of the exploitation of resting-state neurodynamics in disease come from the successful example of treatment of the symptom of fatigue in the context of MS. In fatigued MS patients, the resting-state neurodynamics displayed alterations (Porcaro et al. 2019) supporting the suitability of an ad hoc developed compensatory personalized neuromodulation treatment (Tecchio et al. 2014; Cancelli et al. 2018), which, consistently, induced a normalization of such alterations together with a significant reduction in fatigue levels.

Cortical Neuronal Pools Assessment by Noninvasive EEG

The consistency of the current results with those of the noninvasive study (Cottone et al. 2017a) where M1 and S1 were obtained by the Functional Source Separation (FSS) (Barbati et al. 2006; Tecchio et al. 2007) underlines the ability of this identification algorithm to correctly separate 2 contiguous cortical parcels. Leveraging on the best of noninvasive electrophysiological investigation tools of brain activity (EEG, magnetoencephalography—MEG), FSS assesses intracerebral neuronal activity based on the temporal behavior of the source. Interestingly, FSS exploits specific event-related functional characteristics typical of the cortical region to be identified, providing a tool to assess its local neurodynamics under other behavioral conditions, including the resting-state.

Limitations of the Study

The nonuniform distribution of available channels across subjects, secondary to the epileptogenic region locations, together with the requirement to assess diverse cortical regions in the same subject determined the relatively small dataset selected here.

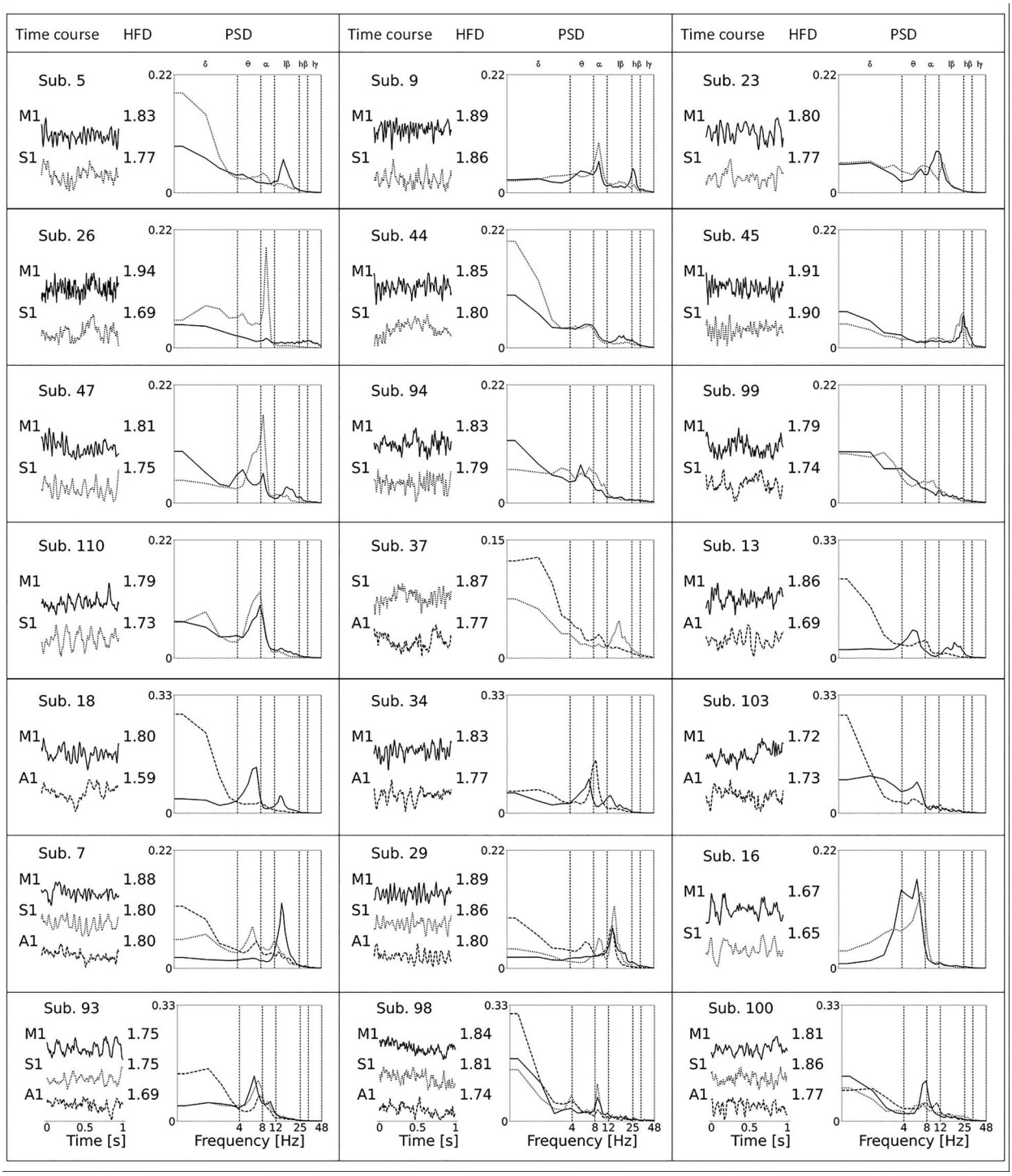

Figure 9. Local neurodynamics in individual subjects. Representation of sEEG time course, power spectral density (PSD) and Higuchi fractal dimension (HFD) in each of the 21 subjects included in the study for the S1 (dotted line), M1 (continuous line), and A1 (dashed line) brain regions. In the panel of each subject, the plot on the left shows a sample (1 s long) of the time series of the cortical area channels (amplitude is normalized to [−1, 1] with the scaler factor given in Table 2) together with the relative estimated HFD value. On the right plot of each panel, normalized PSD versus frequency is presented, where vertical lines separate distinct spectral bands: δ [≤3 Hz], θ [4–7 Hz], α [8–12 Hz], lβ [13–25 Hz], hβ [26–32 Hz], and lγ [33–48 Hz].

About the neuronal activity assessment, it should be considered that the advantage in terms of physiological state investigation via sEEG recordings outside the operating room, is strongly limited by the patient being literally tethered to bed for the days of recordings, due to the large number of wires connecting the implanted electrodes to the recording rig (Parvizi and Kastner 2018).

A further limitation concerns the nature of sEEG signals analyzed in the present study, coming from subjects diagnosed with severe epilepsy. In fact, nowadays the view of epilepsy as a focal

pathology is being overcome, in favor of the understanding of its nature as a network pathology given the core characteristics of altered connectivity patterns between epileptogenic areas and the structures linked to them (Kramer et al. 2011; Proix et al. 2014; Bartolomei et al. 2017; Besson et al. 2017; Devinsky et al. 2018; Lagarde et al. 2018). In terms of the present data, it is plausible to expect that the alterations in neurodynamics related to the epileptogenic cluster would also variably involve other connected—here investigated—areas.

Furthermore, the sample herein analyzed presented nonhomogeneous characteristics in relation to age (from 13 to 68 years old). This feature is expected to generate part of the variability in the local neurodynamics. In fact, in the life span of healthy subjects, the brain complexity hugely modifies both structurally (Marzi et al. 2020) and functionally (Zappasodi et al. 2015; Smits et al. 2016).

Notes

The authors are sincerely grateful to all those who contributed in making this dataset available.

Conflict of Interest: None declared.

Funding

The author(s) received no financial support for the research, authorship, and/or publication for this article.

References

Barbati G, Sigismondi R, Zappasodi F, Porcaro C, Graziadio S, Valente G, Balsi M, Rossini PM, Tecchio F. 2006. Functional source separation from magnetoencephalographic signals. *Hum Brain Mapp*. 27:925–934.

Bartolomei F, Lagarde S, Wendling F, McGonigal A, Jirsa V, Guye M, Bénar C. 2017. Defining epileptogenic networks: contribution of SEEG and signal analysis. *Epilepsia*. 58:1131–1147.

Bassett DS, Sporns O. 2017. Network neuroscience. *Nat Neurosci*. 20:353–364.

Berger H. 1929. Über das Elektrenkephalogramm des Menschen. *Arch Psychiatr Nervenkr*. 87:527–570.

Besson P, Bandt SK, Proix T, Lagarde S, Jirsa VK, Ranjeva JP, Bartolomei F, Guye M. 2017. Anatomic consistencies across epilepsies: a stereotactic-EEG informed high-resolution structural connectivity study. *Brain*. 140:2639–2652.

Brodmann K. 1909. *Vergleichende Lokalisationslehre Der Grosshirnrinde in Ihren Prinzipien Dargestellt Auf Grund Des Zellenbaues*. Leipzig: J.A. Barth.

Bullmore E, Barnes A, Bassett DS, Fornito A, Kitzbichler M, Meunier D, Suckling J. 2009. Generic aspects of complexity in brain imaging data and other biological systems. *Neuroimage*. 47:1125–1134.

Buzsáki G, Logothetis N, Singer W. 2013. Scaling brain size, keeping timing: evolutionary preservation of brain rhythms. *Neuron*. 80:751–764.

Buzsáki G, Mizuseki K. 2014. The log-dynamic brain: how skewed distributions affect network operations. *Nat Rev Neurosci*. 15:264–278.

Buzsáki G, Watson BO. 2012. Brain rhythms and neural syntax: implications for efficient coding of cognitive content and neuropsychiatric disease. *Dialogues Clin Neurosci*. 14:345–367.

Cajal RY. 1888. Estructura de los centros nerviosos de las aves. *Rev Trimest Histol Norm y Patológica*. 1:1–10.

Cancelli A, Cottone C, Giordani A, Migliore S, Lupoi D, Porcaro C, Mirabella M, Rossini PM, Filippi MM, Tecchio F. 2018. Personalized, bilateral whole-body somatosensory cortex stimulation to relieve fatigue in multiple sclerosis. *Mult Scler J*. 24:1366–1374.

Clark A. 2016. *Surfing uncertainty: prediction, action and the embodied mind*. Oxford: Oxford University Press.

Cottone C, Porcaro C, Cancelli A, Olejarczyk E, Salustri C, Tecchio F. 2017. Neuronal electrical ongoing activity as a signature of cortical areas. *Brain Struct Funct*. 222:2115–2126.

Damborská A, Tomescu MI, Honzírková E, Barteček R, Hořínková J, Fedorová S, Ondruš Š, Michel CM. 2019. EEG resting-state large-scale brain network dynamics are related to depressive symptoms. *Front Psychiatry*. 10:548.

Deco G, Jirsa VK, McIntosh AR. 2011. Emerging concepts for the dynamical organization of resting-state activity in the brain. *Nat Rev Neurosci*. 12:43–56.

Devinsky O, Vezzani A, O'Brien TJ, Jette N, Scheffer IE, De Curtis M, Perucca P. 2018. Epilepsy. *Nat Rev Dis Prim*. 4:1–24.

Di Ieva A, Grizzi F, Jelinek H, Pellionisz AJ, Losa GA. 2014. Fractals in the neurosciences, part I: general principles and basic neurosciences. *Neuroscientist*. 20:403–417.

Fox MD, Raichle ME. 2007. Spontaneous fluctuations in brain activity observed with functional magnetic resonance imaging. *Nat Rev Neurosci*. 8:700–711.

Frauscher B, Von Ellenrieder N, Zelmann R, Doležalová I, Minotti L, Olivier A, Hall J, Hoffmann D, Nguyen DK, Kahane P, et al. 2018. Atlas of the normal intracranial electroencephalogram: neurophysiological awake activity in different cortical areas. *Brain*. 141:1130–1144.

Friston K. 2010. The free-energy principle: a unified brain theory? *Nat Rev Neurosci*. 11:127–138.

Gianni E, Bertoli M, Simonelli I, Paulon L, Tecchio F, Pasqualetti P. 2021. tDCS randomized controlled trials in no-structural diseases: a quantitative review. *Sci Rep*. 11:16311.

Golgi C. 1873. Sulla struttura della sostanza grigia del cervello. *Gazz Med Ital*. 33:244–246.

Higuchi T. 1988. Approach to an irregular time series on the basis of the fractal theory. *Phys D Nonlinear Phenom*. 31:277–283.

Johansson RS, Westling G, Bäckström A, Randall FJ. 2001. Eye-hand coordination in object manipulation. *J Neurosci*. 21:6917–6932.

Kopell NJ, Gritton HJ, Whittington MA, Kramer MA. 2014. Beyond the connectome: the dynome. *Neuron*. 83:1319–1328.

Kramer MA, Eden UT, Lepage KQ, Kolaczyk ED, Bianchi MT, Cash SS. 2011. Emergence of persistent networks in long-term intracranial eeg recordings. *J Neurosci*. 31:15757–15767.

Lagarde S, Roehri N, Lambert I, Trebuchon A, McGonigal A, Carron R, Scavarda D, Milh M, Pizzo F, Colombet B, et al. 2018. Interictal stereotactic-EEG functional connectivity in refractory focal epilepsies. *Brain*. 141:2966–2980.

Lin A, Liu KKL, Bartsch RP, Ivanov PC. 2020. Dynamic network interactions among distinct brain rhythms as a hallmark of physiologic state and function. *Commun Biol*. 3(1):197.

Lopes Da Silva FL. 2011. *Niedermeyer's electroencephalography: basic principles, clinical applications and related fields*. 6th ed. Philadelphia: Lippincott Williams & Wilkins.

Marino M, Liu Q, Samogin J, Tecchio F, Cottone C, Mantini D, Porcaro C. 2019. Neuronal dynamics enable the functional differentiation of resting state networks in the human brain. *Hum Brain Mapp*. 40:1445–1457.

Marzi C, Giannelli M, Tessa C, Mascalchi M, Diciotti S. 2020. Toward a more reliable characterization of fractal properties of the cerebral cortex of healthy subjects during the lifespan. *Sci Rep*. 10:16957.

Parvizi J, Kastner S. 2018. Promises and limitations of human intracranial electroencephalography. *Nat Neurosci*. 21:474–483.

Porcaro C, Cottone C, Cancelli A, Rossini PM, Zito G, Tecchio F. 2019. Cortical neurodynamics changes mediate the efficacy of a personalized neuromodulation against multiple sclerosis fatigue. *Sci Rep*. 9(1):18213.

Proix T, Bartolomei F, Chauvel P, Bernard C, Jirsa VK. 2014. Permittivity coupling across brain regions determines seizure recruitment in partial epilepsy. *J Neurosci*. 34:15009–15021.

Razza LB, De Smet S, Moffa A, Sudbrack-Oliveira P, Vanderhasselt MA, Brunoni AR. 2021. Follow-up effects of transcranial direct current stimulation (tDCS) for the major depressive episode: a systematic review and meta-analysis. *Psychiatry Res*. 302:114024.

Smits FM, Porcaro C, Cottone C, Cancelli A, Rossini PM, Tecchio F. 2016. Electroencephalographic fractal dimension in healthy ageing and Alzheimer's disease. *PLoS One*. 11(2):e0149587.

Spetsieris PG, Ko JH, Tang CC, Nazem A, Sako W, Peng S, Ma Y, Dhawan V, Eidelberg D. 2015. Metabolic resting-state brain networks in health and disease. *Proc Natl Acad Sci U S A*. 112:2563–2568.

Tecchio F, Bertoli M, Gianni E, L'Abbate T, Paulon L, Zappasodi F. 2020. To be is to become. Fractal neurodynamics of the body-brain control system. *Front Physiol*. 11:609768.

Tecchio F, Cancelli A, Cottone C, Zito G, Pasqualetti P, Ghazaryan A, Rossini PM, Filippi MM. 2014. Multiple sclerosis fatigue relief by bilateral somatosensory cortex neuromodulation. *J Neurol*. 261:1552–1558.

Tecchio F, Porcaro C, Barbati G, Zappasodi F. 2007. Functional source separation and hand cortical representation for a brain-computer interface feature extraction. *J Physiol*. 580:703–721.

Thut G, Miniussi C, Gross J. 2012. The functional importance of rhythmic activity in the brain. *Curr Biol*. 22:R658–R663.

Wolpert DM, Diedrichsen J, Flanagan JR. 2011. Principles of sensorimotor learning. *Nat Rev Neurosci*. 12: 739–751.

Zappasodi F, Marzetti L, Olejarczyk E, Tecchio F, Pizzella V. 2015. Age-related changes in electroencephalographic signal complexity. *PLoS One*. 10:e0141995.

Zappasodi F, Olejarczyk E, Marzetti L, Assenza G, Pizzella V, Tecchio F. 2014. Fractal dimension of EEG activity senses neuronal impairment in acute stroke. *PLoS One*. 9:e100199.